COMPDYN 2011
III ECCOMAS Thematic Conference on
Computational Methods in Structural Dynamics and Earthquake Engineering
M. Papadrakakis, M. Fragiadakis, V. Plevris (eds.)
Corfu, Greece, 25–28 May 2011

AN EFFICIENT BEAM-COLUMN ELEMENT FOR NONLINEAR 3D FRAME ANALYSIS

Svetlana M. Kostic[1], Prof. Filip C. Filippou[2] and Chin-Long Lee[3]

[1] Faculty of Civil Engineering, University of Belgrade
Bulevar Kralja Aleksandra 73, Belgrade, Serbia
svetlana@grf.bg.ac.rs

[2] Department of Civil and Env. Engineering, University of California
Berkeley, CA 94720 - 1710
filippou@ce.berkeley.edu

[3] Simpson Gumpertz & Heger Inc, 41 Seyon Street
Waltham, MA 02453
clee@sgh.com

Keywords: Nonlinear Analysis, Beam-Column Element, Resultant Plasticity, Generalized Plasticity.

Abstract. *A three-dimensional nonlinear beam-column element for the simulation of the global and local response of frames under monotonic and cyclic loading conditions is presented. The element belongs to the group of concentrated plasticity models, with plastic hinges located at the ends of the element and described with yield and limit surfaces. The concept of generalized plasticity, originally developed for material plasticity, is extended to force resultants in the element formulation. The element takes into account the interaction of the axial force and the bending moments about the principal axes of the cross section and the hardening behavior. The gradual yielding of the cross section is described by the asymptotical approaching of the limit surface.*

1 INTRODUCTION

The adoption of performance-based guidelines for the earthquake resistant design of structures encourages the use of nonlinear analysis methods in professional engineering practice, since it provides more detailed information about the structural response, such as inelastic deformations, than traditional design procedures. Besides the need for a more accurate evaluation method, it is equally important to assess the efficiency and cost of the analysis, which directly, depends on the efficiency and cost of the deployed nonlinear elements. Because of the good compromise between accuracy and computational efficiency, frame elements are commonly used in earthquake engineering practice. In this context distributed inelasticity beam-column elements with integration of the inelastic material response over the cross-section, commonly called fiber beam-column elements, offer a high level of accuracy and flexibility in modeling the 3d inelastic response of structural members, but are computationally expensive, and put high demands on computer storage and memory. Consequently, more economical point hinge models are still widely used for the simulation of the hysteretic response of frames.

To date, many studies have been conducted on concentrated plasticity (or point hinge) beam-column elements [1-6]. The resultant plasticity beam-column elements use concepts of plasticity theory to describe the relation between basic element forces and deformations. The interaction of the axial force and bending moments about the principal axes of the cross section is described by a stress-resultant yield surface, which will be called yield surface in the following presentation. Yield surface equations for different types of cross sections are available [1, 7-9]. Also, different strategies have been proposed for approaching the yield surface and preventing the element force path from drifting away from it. Orbison [1] used a single polynomial expression for the yield surface and developed a five step procedure for mapping the element forces onto the yield surface. The algorithm has some limitations such as the need to subdivide each increment into several sub-increments in order to prevent large errors. Also, the element response can represent an elastic-perfectly plastic material, but not a material with hardening and it does not account for gradual yielding, since the element ends are either fully elastic or fully plastic.

Several models that improve the shortcomings of Orbison's model were proposed in the last 15 years. The idea of loading and bounding surfaces, introduced by Dafalias and Popov [10] for material plasticity, has been successfully applied to the concentrated and distributed plasticity beam-column elements [4, 5, 11-13]. In these models, the loading and bounding surfaces have the same shape, in order to prevent the two surfaces from overlapping. Once the force point touches the bounding surface (at point A), with continued plastic loading, the force point moves along the line that connects the point A and its conjugate point A' that lies on the bounding surface.

A different algorithm for the gradual, asymptotical approach of the bounding surface for the material plasticity was proposed in the generalized plasticity model by Lubliner and Aurichio [14-16]. The model is simple, does not require an expression for the bounding surface and has a straightforward implementation. It introduces two parameters with clear physical meaning β and δ. With the implementation of the return mapping algorithm, it is computationally very efficient.

The element in this paper adopts the idea of the generalized plasticity material model. The backward-Euler algorithm with general closest point projection [17] is modified to suit the element-based force-deformation relationship. Isotropic and kinematic hardening (or softening) is possible. Because of its quadratic convergence and simplicity, the element is computationally very efficient and overcomes shortcoming of elastic-perfectly plastic elements.

2 ELEMENT FORMULATION

2.1 Basic Framework

The underlying assumption of the generalized plasticity theory is the existence of two continuous real valued functions, the limit function F and yield function f [15, 16]. The yield function f encloses the region with elastic behavior forming the boundary between elastic and inelastic region:

$$f < 0 \Rightarrow \text{elastic state} - \text{no inelastic effects}$$
$$f \geq 0 \Rightarrow \text{inelastic state} - \text{inelastic effects may or may not occur depending on loading or unloading}$$

The basic forces **q** of a three-dimensional (3d) frame element without rigid body modes are shown in Figure 1. The corresponding deformations are denoted with **v**. Zero-length plastic hinges may form at one or both element ends, while the rest of the element is elastic.

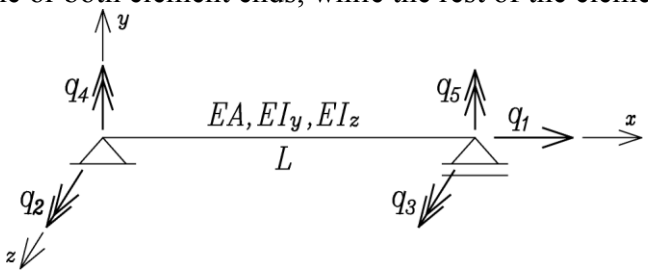

Figure 1: Basic element forces **q**.

In beam-column stress-resultant plasticity elements the classical material plasticity rules are modified to represent the axial force, bending moment interaction under inelastic behavior. Therefore, the following equations, that govern the element behavior, are assumed:

1. The element deformations **v** are decomposed into the linear elastic contribution $\mathbf{v^e}$ and the plastic contribution $\mathbf{v^p}$:

$$\mathbf{v} = \mathbf{v^e} + \mathbf{v^p} \tag{1}$$

2. There is a linear elastic relation between basic forces and elastic element deformations:

$$\mathbf{q} = \mathbf{k_e}\mathbf{v^e} = \mathbf{k_e}\left(\mathbf{v} - \mathbf{v^p}\right) \tag{2}$$

where $\mathbf{k_e}$ is the elastic element stiffness matrix.

3. The yield function f is expressed in terms of the basic element forces **q**, of vector **a** which defines the position of the center of the surface and a hardening variable α which models isotropic hardening. H_{iso} and H_{kin} are the isotropic and kinematic plastic hardening (or softening) non-dimensional parameters, respectively. The yield function f distinguishes between elastic and inelastic states.

$$f(\mathbf{q}, \mathbf{a}, \alpha) = \Phi(\mathbf{q} - \mathbf{a}) - H_{iso}\alpha \tag{3}$$

4. The limit function F depends on the nonnegative consistency parameter λ and has the following form proposed for generalized plasticity models:

$$F = h(f)\frac{d}{dt}(\Phi) - \lambda \tag{4}$$

$$h(f) = \frac{f}{\delta(\beta - f) + (H_{iso} + H_{kin})\beta} \tag{5}$$

where δ and β are two non dimensional positive constants (δ measures the speed of approach of the model to the asymptotic behavior, and β measures the distance between the current and the asymptotic yield function). The meaning of surfaces and parameters δ and β is shown in Fig.2.

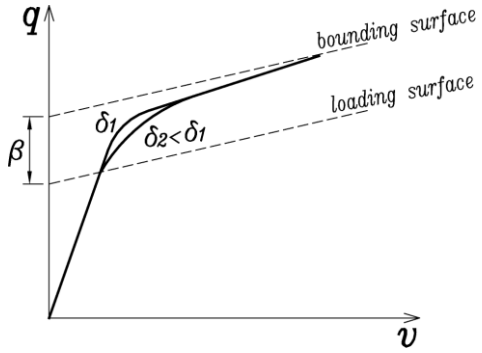

Figure 2: Basic force **q** versus generalized element deformation **v**.

5. An associative plastic flow rule is assumed that is described with the following equation:

$$\dot{\mathbf{v}}^{\mathbf{p}} = \lambda \frac{\partial f}{\partial \mathbf{q}}. \tag{6}$$

6. The surface motion (kinematic hardening mechanism) is defined by Ziegler's rule:

$$\dot{\mathbf{a}} = H_{kin}\mathbf{\Pi}\dot{\mathbf{v}}^{\mathbf{p}} = H_{kin}\mathbf{\Pi}\lambda \frac{\partial f}{\partial \mathbf{q}}. \tag{7}$$

where $\mathbf{\Pi}$ is a scaling matrix, that accounts for the different dimensions between **a** and $\mathbf{v}^{\mathbf{p}}$ and is adopted here equal to:

$$\mathbf{\Pi} = diag\left\{\frac{EA}{L}, \frac{EI_z}{L}, \frac{EI_z}{L}, \frac{EI_y}{L}, \frac{EI_y}{L}\right\}. \tag{8}$$

7. The simplest evolutionary equation for α is adopted corresponding to equivalent plastic strain:

$$\dot{\alpha} = \left\|\dot{\mathbf{v}}^{\mathbf{p}}\right\| = \lambda \left\|\frac{\partial f}{\partial \mathbf{q}}\right\|, \tag{9}$$

where:

$$\left\|\frac{\partial f}{\partial \mathbf{q}}\right\| = \left[\left(\frac{\partial f}{\partial \mathbf{q}}\right)^T \mathbf{\Lambda} \frac{\partial f}{\partial \mathbf{q}}\right]^{1/2}, \tag{10}$$

with a scaling matrix $\mathbf{\Lambda}$ defined as:

$$\mathbf{\Lambda} = diag\left\{\frac{1}{L^2}, \mathbf{I_4}\right\}. \tag{11}$$

Matrix $\mathbf{I_4}$ is the 4x4 identity matrix.

8. The Kuhn-Tucker complementarity conditions are:

$$\lambda \geq 0, \quad F \leq 0, \quad \lambda F = 0\,. \tag{12}$$

These conditions reduce the plastic problem to a constrained optimization problem.

9. The limit equation can be written in the following form, *-F=0*:

$$\lambda - h(f)\frac{d}{dt}(\Phi) = 0\,. \tag{13}$$

Integrating this equation over the time interval $[t_n, t_{n+1}]$, we obtain the discrete limit condition:

$$\Delta\lambda - h(f)(\Phi_{n+1} - \Phi_n) = 0\,. \tag{14}$$

2.2 Integration Algorithm

The model in the previous section can be transformed into a discrete constrained optimization problem by applying the backward (implicit) Euler numerical integration scheme.

Assuming that the state of the element is known at time step t_n, means that the values $\{\mathbf{v_n}, \mathbf{v_n^p}, \mathbf{a_n}, \boldsymbol{\alpha_n}\}$ are available. The basic forces are also known since they can be found from equation (2):

$$\mathbf{q_n} = \mathbf{k_e}(\mathbf{v_n} - \mathbf{v_n^p})\,. \tag{15}$$

Suppose that we know an increment in total element deformations $\mathbf{\Delta v}$ at the time step t_{n+1}, so that $\mathbf{v_{n+1} = v_n + \Delta v}$. Other state variables $\mathbf{v_{n+1}^p}$, $\mathbf{a_{n+1}}$ and α_{n+1} should be updated, as well, and this is the problem to be solved.

By applying the backward-Euler method we have:

$$\mathbf{v_{n+1}^p} = \mathbf{v_n^p} + \mathbf{g}_{n+1}(\mathbf{q}_{n+1}, \mathbf{a}_{n+1})\Delta\lambda\,. \tag{16}$$

$$\mathbf{a}_{n+1} = \mathbf{a}_n + H_{kin}\mathbf{\Pi g}_{n+1}(\mathbf{q}_{n+1}, \mathbf{a}_{n+1})\Delta\lambda\,. \tag{17}$$

$$\alpha_{n+1} = \alpha_n + \left\|\mathbf{g}_{n+1}(\mathbf{q}_{n+1}, \mathbf{a}_{n+1})\right\|\Delta\lambda\,. \tag{18}$$

where $\Delta\lambda = \int_{t_n}^{t_{n+1}} \lambda dt$ and $\mathbf{g} = \frac{\partial f}{\partial \mathbf{q}}$. The discrete version of the Kuhn-Tucker conditions (12) is:

$$\Delta\lambda \geq 0, \quad F_{n+1} \leq 0, \quad \Delta\lambda F_{n+1} = 0\,. \tag{19}$$

The discrete system of equations will be solved by the two-step predictor-corrector return mapping algorithm.

2.3 Return Mapping Algorithm

The return mapping algorithm is an efficient and robust integration scheme, which belongs to the family of elastic predictor - plastic corrector algorithms. In the first, predictor step, a purely elastic (trial) state is computed ($\mathbf{q_{n+1}^{trial}}$). If this trial state violates the integrated limit in-

equality $F \leq 0$, the element forces are corrected in the second, corrector, step using the trial state as an initial condition. Otherwise, the second step is skipped and the trial solution represents the solution at t_{n+1}.

Since the element has two nodes, and plastic deformations can occur at both of them, the yield functions f_1 and f_2, limit functions F_1 and F_2, consistency parameters $\Delta\lambda_1$ and $\Delta\lambda_2$ and hardening variables α_1 and α_2 are lumped into vectors $\mathbf{f}$, $\mathbf{F}$, $\mathbf{\Delta\lambda}$ and $\boldsymbol{\alpha}$, respectively. The diagonal 2x2 matrix that has nonzero values on the main diagonal, equal to f_1 and f_2 is denoted as *diag*($\mathbf{f}$), and similarly for others: *diag*($\mathbf{F}$), *diag*($\mathbf{\Delta\lambda}$), etc.

When both plastic hinges form at element ends, $\mathbf{g}$ is a 3x2 matrix, with the first column equal to $\partial_{\mathbf{q}} f_1 = \mathbf{g}_1$ and the second equal to $\partial_{\mathbf{q}} f_2 = \mathbf{g}_2$. If only one node yields, $\mathbf{g}$ is a 3x1 vector and is equal to $\mathbf{g}_1$ or $\mathbf{g}_2$, depending on which node yields. The parameter $\mathbf{\Delta\Delta\lambda}$ for the non-yielding node is zero.

1. Predictor step: We consider a purely elastic step obtained by freezing the plastic flow, so that $\Delta\lambda=0$.

$$\mathbf{q}_{\mathbf{n+1}}^{trial} = \mathbf{k}_e(\mathbf{v}_{n+1} - \mathbf{v}_n^p) \tag{20}$$

$$\mathbf{v}_{n+1}^{p,trial} = \mathbf{v}_n^p \tag{21}$$

$$\mathbf{a}_{n+1}^{trial} = \mathbf{a}_n \tag{22}$$

$$\boldsymbol{\alpha}_{n+1}^{trial} = \boldsymbol{\alpha}_n \tag{23}$$

$$\mathbf{f}_{n+1}^{trial} = \mathbf{f}(\mathbf{q}_{n+1}^{trial}, \mathbf{a}_{n+1}^{trial}, \boldsymbol{\alpha}_{n+1}^{trial}) = \boldsymbol{\Phi}_{n+1}^{trial} - H_{iso}\boldsymbol{\alpha}_{n+1}^{trial} \tag{24}$$

$$\boldsymbol{\Phi}_{n+1}^{trial} = \boldsymbol{\Phi}(\mathbf{q}_{n+1}^{trial} - \mathbf{a}_{n+1}^{trial}) \tag{25}$$

Once the trial state is computed, we check the limit condition $F \leq 0$, which due to $\Delta\lambda=0$, reduces to the condition $\mathbf{f}_{n+1}^{trial}(\boldsymbol{\Phi}_{n+1}^{trial} - \boldsymbol{\Phi}_n) \leq 0$.

If this condition is not violated, the trial state is admissible state and:

$$\mathbf{v}_{n+1}^p = \mathbf{v}_n^p \tag{26}$$

$$\mathbf{a}_{n+1} = \mathbf{a}_n \tag{27}$$

$$\boldsymbol{\alpha}_{n+1} = \boldsymbol{\alpha}_n \tag{28}$$

$$\mathbf{q}_{n+1} = \mathbf{q}_{n+1}^{trial} \tag{29}$$

$$\mathbf{k} = \mathbf{k}_e \tag{30}$$

If the condition $\mathbf{f}_{n+1}^{trial}(\boldsymbol{\Phi}_{n+1}^{trial} - \boldsymbol{\Phi}_n) \leq 0$ is not satisfied, the trial state is nonadmissible state and the correction should be done in the corrector step.

2. Corrector step: We require the residuals $\mathbf{R_{1,n+1}}$, $\mathbf{R_{2,n+1}}$ and $\mathbf{R_{3,n+1}}$ and the limit condition (14) to be zero.

$$\mathbf{R_{1,n+1}} = -\mathbf{v_{n+1}^p} + \mathbf{v_n^p} + \mathbf{g_{n+1}}\mathbf{\Delta\lambda} \tag{31}$$

$$\mathbf{R_{2,n+1}} = -\mathbf{a_{n+1}} + \mathbf{a_n} + H_{kin}\mathbf{\Pi g_{n+1}}\mathbf{\Delta\lambda_{n+1}} \tag{32}$$

$$\mathbf{R_{3,n+1}} = -\boldsymbol{\alpha}_{\mathbf{n+1}} + \boldsymbol{\alpha}_{\mathbf{n}} + \left\|\mathbf{g_{n+1}}\right\|\mathbf{\Delta\lambda_{n+1}} \tag{33}$$

After linearization of equations (31)-(34) and the limit equation (14) and after some numerical manipulations, we get the following nonlinear system of equations for determining the parameter $\mathbf{\Delta\Delta\lambda}$:

$$(\mathbf{a\Delta\Delta\lambda})(\mathbf{b\Delta\Delta\lambda}) + \mathbf{c\Delta\Delta\lambda} + \mathbf{d} = \mathbf{0} \tag{34}$$

The smallest positive solution $\mathbf{\Delta\Delta\lambda}$ (the increment of the consistency parameter in the *k*-th iteration) corresponds to the physically correct solution.
The system can be solved, for example, with the Newton method or another algorithm for a nonlinear equation system. The solution of the linear equation system $\mathbf{c\Delta\Delta\lambda} + \mathbf{d} = 0$ can be used as initial value. The coefficients **a**, **b**, **c** and **d** are:

$$\mathbf{a} = diag(\boldsymbol{\delta}) - \mathbf{\Phi 2} \tag{35}$$

$$\mathbf{b} = \mathbf{f2} \tag{36}$$

$$\begin{aligned}\mathbf{c} = {} & diag(\mathbf{\Delta\lambda\delta})\mathbf{f2} + diag(\boldsymbol{\delta}(\boldsymbol{\beta} - \mathbf{f1}) + (H_{iso} + H_{kin})\boldsymbol{\beta}) + diag(\mathbf{f1})\mathbf{\Phi 2} + \\ & + diag(\mathbf{\Phi 1} - \mathbf{\Phi_n})\mathbf{f2}\end{aligned} \tag{37}$$

$$\mathbf{d} = diag(\mathbf{\Delta\lambda}(\boldsymbol{\delta}(\boldsymbol{\beta} - \mathbf{f1}) + (H_{iso} + H_{kin})\boldsymbol{\beta})) - \mathbf{f1}(\mathbf{\Phi 1} - \mathbf{\Phi}_n) \tag{38}$$

where

$$\mathbf{f1} = \mathbf{f}^{trial} + \mathbf{g}^T(\mathbf{M} - \mathbf{P}) - H_{iso}\mathbf{T} \tag{39}$$

$$\mathbf{f2} = \mathbf{g}^T(\mathbf{N} - \mathbf{S}) - H_{iso}\mathbf{L} \tag{40}$$

$$\mathbf{\Phi 1} = \mathbf{\Phi}^{trial} + \mathbf{g}^T(\mathbf{M} - \mathbf{P}) \tag{41}$$

$$\mathbf{\Phi 2} = \mathbf{g}^T(\mathbf{N} - \mathbf{S}) \tag{42}$$

$$\mathbf{M} = \mathbf{C}(-\mathbf{R}_1 + \mathbf{Q\Delta\Delta\lambda BR}_2) \tag{43}$$

$$\mathbf{N} = \mathbf{C}(\mathbf{g} - \mathbf{Q\Delta\Delta\lambda}H_{kin}\mathbf{\Pi g}) \tag{44}$$

$$\mathbf{P} = \mathbf{B}(\mathbf{R}_2 + H_{kin}\mathbf{\Pi Q\Delta\lambda M}) \tag{45}$$

$$\mathbf{S} = \mathbf{B}H_{kin}\mathbf{\Pi}(\mathbf{Q\Delta\Delta\lambda} - \mathbf{g}) \tag{46}$$

$$\mathbf{T} = \mathbf{R}_3 + \mathbf{\Delta\lambda}(\mathbf{Qn})^T(\mathbf{M} - \mathbf{P}) \tag{47}$$

$$\mathbf{L} = \mathbf{\Delta\lambda}(\mathbf{Qn})^T(\mathbf{N} - \mathbf{S}) - \|\mathbf{g}\| \tag{48}$$

with

$\mathbf{A} = (\mathbf{k}_e^{-1} + \mathbf{Q\Delta\Delta})^{-1}$, $\mathbf{Q} = \partial^2_{\mathbf{qq}}\mathbf{f}$, $\mathbf{B} = (\mathbf{1} + H_{kin}\mathbf{\Pi Q\Delta\lambda})^{-1}$, $\mathbf{n} = \dfrac{\mathbf{\Lambda g}}{\|\mathbf{g}\|}$ and

$\mathbf{C} = (\mathbf{A}^{-1} - \mathbf{Q\Delta\Delta\lambda}H_{kin}\mathbf{\Pi Q\Delta\lambda})^{-1}$. In the equations (34) to (48) the superscript *k*, denoting the iteration, and subscript *n+1*, denoting the value at t_{n+1}, are omitted for simplicity.
For $\boldsymbol{\delta}=\mathbf{0}$ and $H_{iso} = H_{kin} = 0$ the model reduces to elastic-perfectly plastic behavior with the solution:

$$\mathbf{\Delta\Delta\lambda}^{(k)}_{n+1} = \left(\left(\mathbf{g}^{(k)}_{n+1}\right)^T \mathbf{A}^{(k)}_{n+1}\mathbf{g}^{(k)}_{n+1}\right)^{-1}\left(\mathbf{f}^{(k)}_{n+1} - \left(\mathbf{g}^{(k)}_{n+1}\right)^T \mathbf{A}^{(k)}_{n+1}\mathbf{R}^{(k)}_{1,n+1}\right) \tag{49}$$

The elastic-perfectly plastic solution is also recovered when $\boldsymbol{\beta}=\mathbf{0}$ and $H_{iso}=H_{kin}=0$. In the case when only one node yields, the system of nonlinear equations transforms into a single quadratic equation.

After finding the increment $\boldsymbol{\Delta\Delta\lambda}$, either as a solution of a system of nonlinear equations or a single equation, the consistency parameter is updated:

$$\boldsymbol{\Delta\Delta\lambda}_{n+1}^{(k+1)} = \boldsymbol{\Delta\lambda}_{n+1}^{(k)} + \boldsymbol{\Delta\Delta\lambda}_{n+1}^{(k)} \tag{50}$$

2.4 Tangent Stiffness Matrix

The tangent stiffness can be obtained by enforcing the satisfaction of the linearized discrete limit condition. After some manipulation the following expression for the tangent stiffness matrix $\mathbf{k}_{n+1}$ results

$$\begin{aligned}
\mathbf{k}_{n+1} &= \frac{d\mathbf{q}}{d\mathbf{v}}|_{n+1} = \mathbf{C}_{n+1} - \mathbf{N}_{n+1}\left(\mathbf{Y}_{n+1}\right)^{-1}\mathbf{Z}_{n+1} \\
\mathbf{Y}_{n+1} &= diag\left(\boldsymbol{\delta}\left(\boldsymbol{\beta} - \mathbf{f}_{n+1}\right) + \left(H_{iso} + H_{kin}\right)\boldsymbol{\beta}\right) + diag\left(\mathbf{f}_{n+1} + \boldsymbol{\Phi}_{n+1} - \boldsymbol{\Phi}_{n} + \boldsymbol{\Delta\lambda}_{n+1}\boldsymbol{\delta}\right)\mathbf{g}_{n+1}^{T}\mathbf{X}_{2} - \\
&\quad - diag\left(H_{iso}\left(\boldsymbol{\Phi}_{n+1} - \boldsymbol{\Phi}_{n} + \boldsymbol{\Delta\lambda}_{n+1}\boldsymbol{\delta}\right)\right)\mathbf{L}_{n+1} \\
\mathbf{Z}_{n+1} &= diag\left(\mathbf{f}_{n+1} + \boldsymbol{\Phi}_{n+1} - \boldsymbol{\Phi}_{n} + \boldsymbol{\Delta\lambda}_{n+1}\boldsymbol{\delta}\right)\mathbf{g}_{n+1}^{T}\mathbf{X}_{1} - diag\left(H_{iso}\boldsymbol{\Delta\lambda}_{n+1}\boldsymbol{\delta}\right)\boldsymbol{\Delta\lambda}_{n+1}\left(\mathbf{Q}_{n+1}\mathbf{n}_{n+1}\right)^{T}\mathbf{X}_{1} - \\
&\quad - diag\left(H_{iso}\left(\boldsymbol{\Phi}_{n+1} - \boldsymbol{\Phi}_{n}\right)\right)\boldsymbol{\Delta\lambda}_{n+1}\left(\mathbf{Q}_{n+1}\mathbf{n}_{n+1}\right)^{T}\mathbf{X}_{1}
\end{aligned} \tag{51}$$

We used the substitutions $\mathbf{X_1}$ and $\mathbf{X_2}$ with the following definition

$$\begin{aligned}
\mathbf{X}_{1} &= \mathbf{C}_{n+1} - \mathbf{B}_{n+1}H_{kin}\boldsymbol{\Pi}\mathbf{Q}_{n+1}\boldsymbol{\Delta\lambda}_{n+1}\mathbf{C}_{n+1} \\
\mathbf{X}_{2} &= \mathbf{N}_{n+1} - \mathbf{S}_{n+1}
\end{aligned} \tag{52}$$

As for the consistency parameter $\boldsymbol{\Delta\Delta\lambda}$, for parameters $\boldsymbol{\delta}=\mathbf{0}$ and $H_{iso}=H_{kin}=0$ or $\boldsymbol{\beta}=\mathbf{0}$ and $H_{iso}=H_{kin}=0$, the consistent tangent stiffness matrix reduces to the expression for the elastic-perfectly plastic case:

$$\mathbf{k}_{n+1} = \mathbf{A}_{n+1} - \mathbf{A}_{n+1}\mathbf{g}_{n+1}\left(\mathbf{g}_{n+1}^{T}\mathbf{A}_{n+1}\mathbf{g}_{n+1}\right)^{-1}\mathbf{g}_{n+1}^{T}\mathbf{A}_{n+1} \tag{53}$$

3 NUMERICAL EXAMPLES

To verify the capabilities of the new element, two simple examples are studied. The response of the new element, named GPMNYS element (from Generalized Plasticity N-M Yield Surface), is compared with the solution of the elastic-perfectly plastic concentrated plasticity element (EPPNMYS element) [18] and the fiber hinge element [19] whose solution is denoted as FIBER and represents the benchmark solution. FEDEASLab, a Matlab toolbox for nonlinear static and dynamic analysis [20], was used for the simulation.

3.1 Cantilever Column

The first example refers to the cantilever column shown in Figure 3(a) which is used before in a study of efficient cross section discretization of fiber beam-column element [21]. In tests B6 and B8_7, the column was subjected to uniaxial and biaxial tip translation history with variable axial force (Figure 3(b-c)). In Test B6, the column tip is subjected to lateral displacements in the strong axis direction, with variation of axial force between -0.05Np and -0.45Np. In Test B8_7, the column tip is subjected to displacements in the Y and Z directions so that normalized bending moments about strong and weak axis are in the ratio 0.5, with variation of axial force between -0.05Np and -0.45Np.

The response of a homogeneous column with elastic perfectly plastic material, obtained with the distributed inelasticity fiber model with fine section discretization (108 fibers) and five Gauss-Lobatto integration points along its length, is compared with the response of the two concentrated plasticity elements, GPNMYS and EPPNMYS elements.

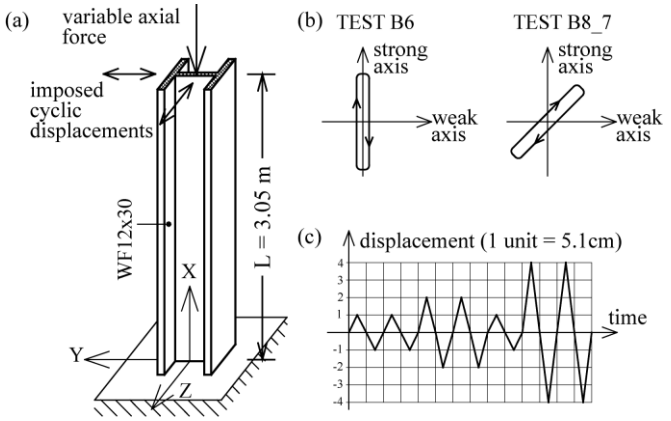

Figure 3: (a) Cantilever column; (b) B6 and B8_7 tip displacement pattern; (c) tip displacement history.

The assumed yield function, i.e. N-M_z-M_y interaction curve, for each end of the beam is:

$$f(p,m_z,m_y)=1.15p^2+m_z^2+m_y^4+3.67p^2m_z^2+3p^6m_y^2+4.65m_z^4m_y^2-c \qquad (54)$$

Where p is the normalized axial force $p=(N-a_p)/N_p$ and $m_z=(M_z-a_z)/M_{pz}$ and $m_y=(M_y-a_y)/M_{py}$, respectively, are the normalized bending moment about strong and weak axis. The variables a_p, a_z and a_y are components of the vector that describes the dispacement of the yield surface in the N-M_z-M_y space due to kinematic hardening mechanism. The variable c determines dimensions of the yield surface. Coefficients in the equation (54) are determined to fit the best yield surface for W12x30 US steel cross section with *c=1.0* [1]. In GPNMYS and EPPNMYS models, both nodes are assumed to have the same properties. The coefficient c is taken equal to *0.3* in GPNMYS and *1.0* in EPPNMYS model. Additional parameters of the GPNMYS model are: $\delta=0.15$, $\beta=0.70$ and $H_{iso}=H_{kin}=0$. The results are shown in Figures 4-5 for Test B6 and in Figures 6-9 for Test B8_7.

It should be emphasized that the elapsed time during these tests were, approximately, in the ratio 1:1.15:21 for EPPNMYS: GPNMYS: FIBER element, respectively.

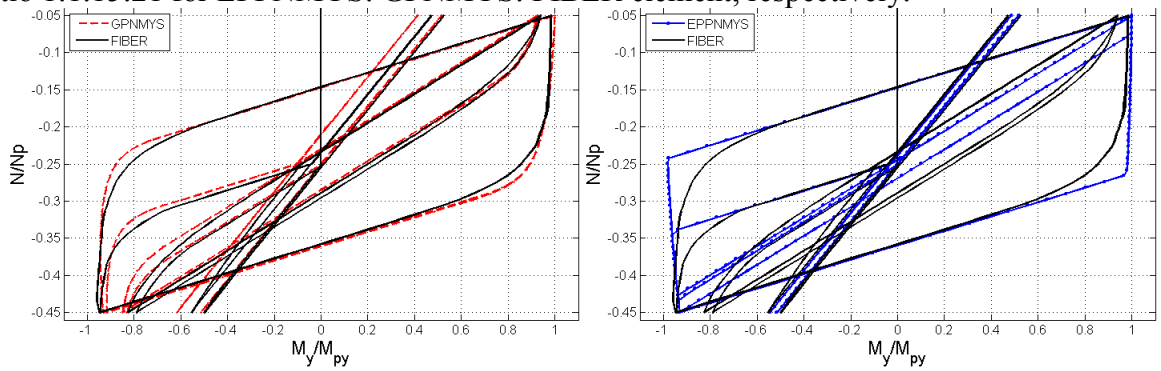

Figure 4: Test B6: normalized bending moment – normalized axial force path
(a) GPNMYS and FIBER; (b) EPPNMYS and FIBER element.

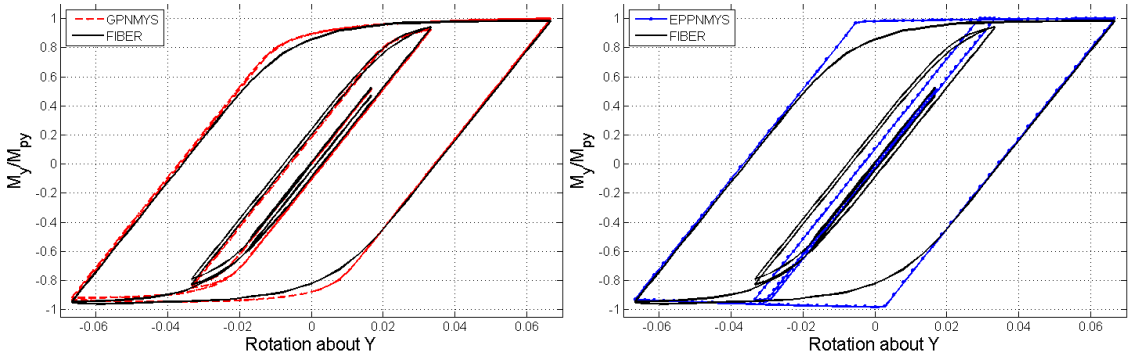

Figure 5: Test B6: normalized bending moment – rotation relation
(a) GPNMYS and FIBER; (b) EPPNMYS and FIBER element.

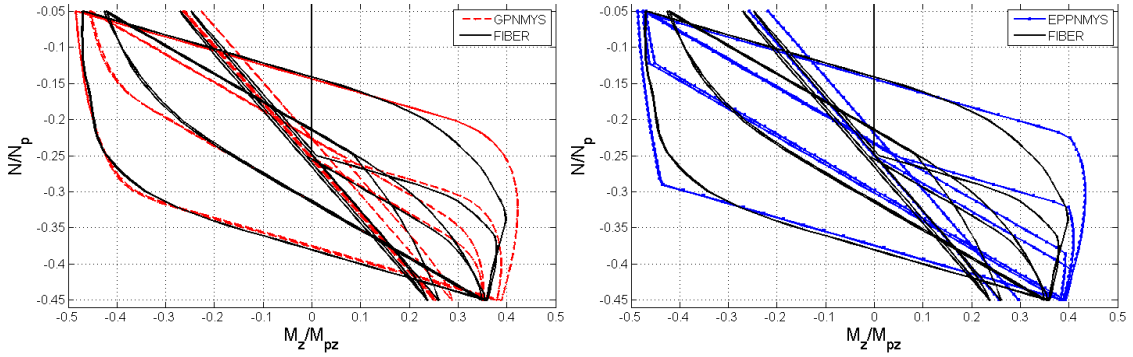

Figure 6: Test B8_7: normalized bending moment about Z – normalized axial force path
(a) GPNMYS and FIBER; (b) EPPNMYS and FIBER element.

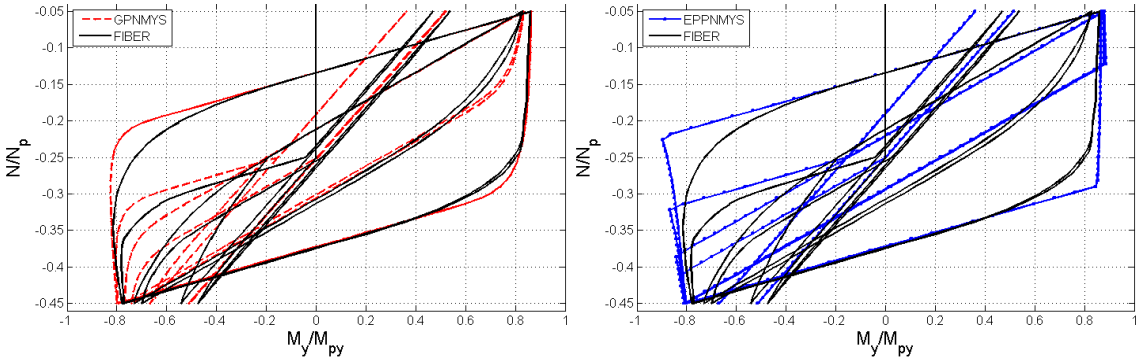

Figure 7: Test B8_7: normalized bending moment about Y – normalized axial force path
(a) GPNMYS and FIBER; (b) EPPNMYS and FIBER element.

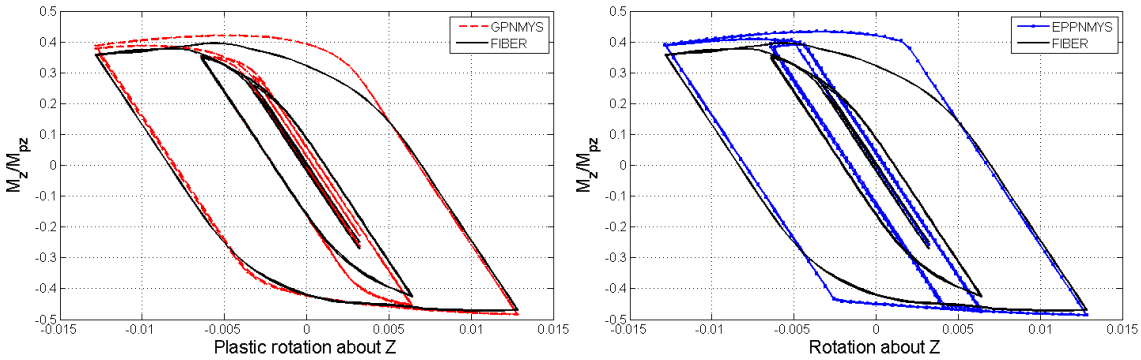

Figure 8: Test B8_7: normalized bending moment about Z – rotation relation
(a) GPNMYS and FIBER; (b) EPPNMYS and FIBER element.

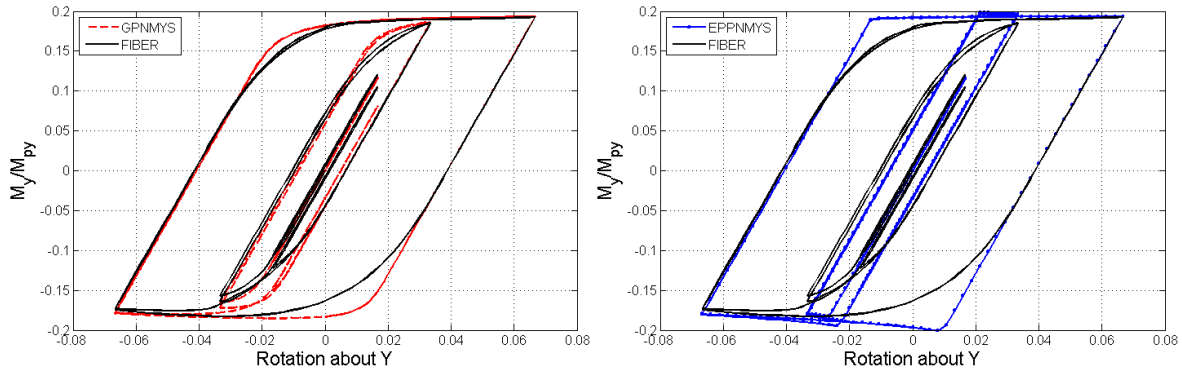

Figure 9: Test B8_7: normalized bending moment about Y – rotation relation
(a) GPNMYS and FIBER; (b) EPPNMYS and FIBER element.

To verify the capabilities of the GPNMYS element to simulate hardening behavior, the Test B6 is conducted again. The material is assumed to have 3% kinematic hardening in FIBER model. Parameter H_{kin} of the GPNMYS model is taken equal to *0.08*, while other parameters are the same as in the Test B6 without hardening. Results are shown in Figure 10.

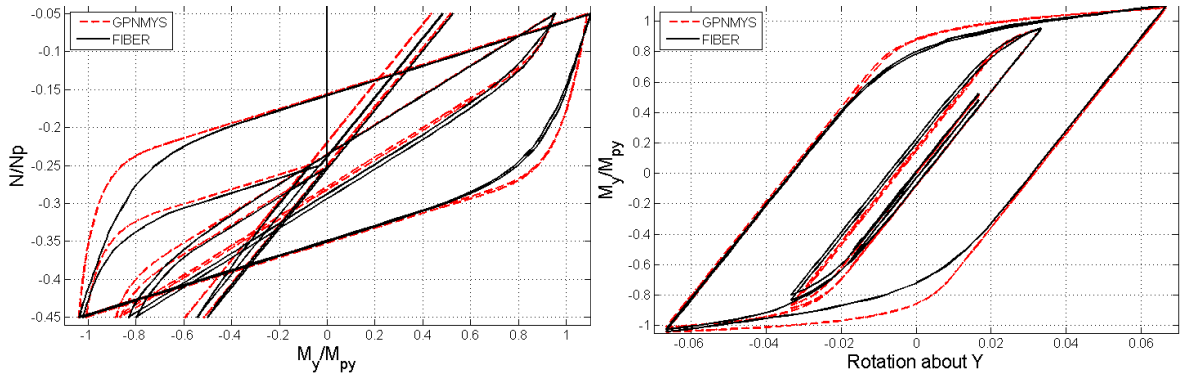

Figure 10: Test B6 with hardening - GPNMYS and FIBER element: (a) normalized bending moment – normalized axial force path; (b) normalized bending moment about Y – rotation relation.

3.2 Portal frame example

The second example refers to the portal frame shown in Figure 11, previously studied by El-Zanaty [22]. Gravity loads are applied first and then kept constant wile lateral load is gradually increasing. The residual stresses are not considered since this effect cannot be captured with the EPPNMYS element. In the GPNMYS element this effect can be included by specifying the size of the elastic domain (loading surface) [23].

The nonlinear geometry under large displacements is accounted for with the corotational formulation [24]. In each of the three models (GPNMYS, EPPNMYS and fiber) each member of the portal frame is represented with one element. The material model is assumed elastic-perfectly plastic. Three different levels of vertical load are studied: 20%, 40% and 60% of the ultimate vertical load of the frame and results for bending about the major axis are given in Figure 12.

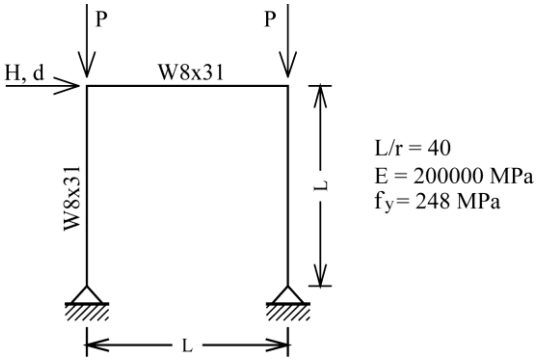

Figure 11: El-Zanaty portal frame.

The following yield function is used:

$$f(p,m_z) = p^2 + m_z^2 + 3.5p^2m_z^2 - c \tag{55}$$

Where p and m_z are as defined before. The parameter c equal to *1.0* is used in EPPNMYS element, and *c=0.71* for GPNMYS element. Additional parameters of the GPNMYS model are: δ*=0.1*, β*=0.27*.

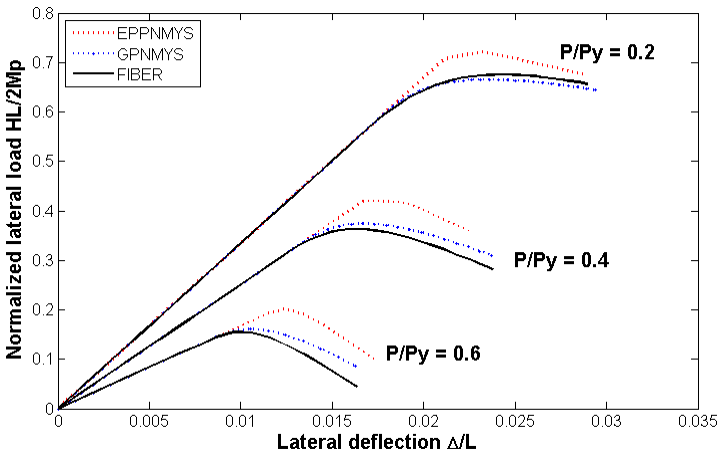

Figure 13: Load-displacement response of El-Zanaty frame.

As can be seen from the results, the response of the GPNMYS element is closer to the exact – FIBER solution due to its capability to describe the gradual yielding of the cross section.

4 CONCLUSION

In the paper, a new three-dimensional nonlinear beam-column element, called GPNMYS, for the simulation of the global and local response of frames under monotonic and cyclic loading conditions is presented. The element belongs to the family of concentrated plasticity elements, with plastic hinges located at the ends of the element and described with yield and limit surfaces. The concepts of generalized material plasticity are extended to force resultants and used in the element formulation. The element takes into account the interaction of the axial force and the bending moments about the principal axes of the cross section and the hardening behavior. The gradual yielding of the cross section is described by the asymptotical approach to the limit surface. The model is relatively simple and introduces parameters with clear physical meaning. With the implementation of the return mapping algorithm and quadratic convergence it is, also, computationally very efficient.

The capability of the new GPNMYS element is verified with two examples by comparing its response with that of an elastic perfectly plastic element resultant plasticity element, which is also based on the return map algorithm, and with the results of a fiber beam-column element. In comparison with perfectly-plastic element, the GPNMYS element proves significantly more versatile in the simulation of frame response under complex loading conditions without significant increase in calculation time, which remains equal to approximately 15% of the time required by the fiber beam-column with an adequate level of discretization.

ACKNOWLEDGEMENTS

The first author thanks the Ministry of Science of the Republic of Serbia for financial support under project TR36046.

REFERENCES

[1] J. G. Orbison, *et al.*, "Yield surface applications in nonlinear steel frame analysis," *Computer Methods in Applied Mechanics and Engineering,* vol. 33, pp. 557-573, 1982.

[2] S. I. Hilmy and J. F. Abel, "Material and geometric nonlinear dynamic analysis of steel frames using computer graphics," *Computers & Structures,* vol. 21, pp. 825-840, 1985.

[3] G. H. Powell and P. F.-S. Chen, "3D Beam-Column Element with Generalized Plastic Hinges," *Journal of Engineering Mechanics,* vol. 112, pp. 627-641, 1986.

[4] J. F. Hajjar and B. C. Gourley, "A cyclic nonlinear model for concrete-filled tubes. I: Formulation," *Journal of Structural Engineering,* vol. 123, p. 736, 1997.

[5] J. F. Hajjar and B. C. Gourley, "A cyclic nonlinear model for concrete-filled tubes. II: Verification," *Journal of Structural Engineering,* vol. 123, p. 745, 1997.

[6] C. K. Iu, *et al.*, "Second-order inelastic analysis of composite framed structures based on the refined plastic hinge method," *Engineering Structures,* vol. 31, pp. 799-813, 2009.

[7] S. Kitipornchai, *et al.*, "Single-equation yield surfaces for monosymmetric and asymmetric sections," *Engineering Structures,* vol. 13, pp. 366-370, 1991.

[8] B. Skallerud, "Yield surface formulations for eccentrically loaded planar bolted or welded connections," *Computers & Structures,* vol. 48, pp. 811-818, 1993.

[9] W. F. Chen and T. Atsuta, *Theory of Beam-Columns*. New York: McGraw Hill, 1977.

[10] Y. F. Dafalias and E. P. Popov, "Cyclic loading for materials with a vanishing elastic region," *Nuclear Engineering and Design,* vol. 41, pp. 293-302, 1977.

[11] S. El-Tawil and G. G. Deierlein, "NONLINEAR ANALYSIS OF MIXED STEEL-CONCRETE FRAMES. II: IMPLEMENTATION AND VERIFICATION," *Journal of Structural Engineering,* vol. 127, p. 656, 2001.

[12] S. El-Tawil and G. G. Deierlein, "NONLINEAR ANALYSIS OF MIXED STEEL-CONCRETE FRAMES. I: ELEMENT FORMULATION," *Journal of Structural Engineering,* vol. 127, p. 647, 2001.

[13] J. Jin and S. El-Tawil, "Inelastic Cyclic Model for Steel Braces," *Journal of Engineering Mechanics, ASCE,* vol. 129, pp. 548-557, May 2003 2003.

[14] J. Lubliner, *et al.*, "A New Model of Generalized Plasticity and Its Numerical Implementation," *International Journal of Solids and Structures,* vol. 30, pp. 3171-3184, 1993.

[15] F. Auricchio and R. L. Taylor, "2 Material Models for Cyclic Plasticity - Nonlinear Kinematic Hardening and Generalized Plasticity," *International Journal of Plasticity,* vol. 11, pp. 65-98, 1995.

[16] F. Auricchio and R. L. Taylor, "A generalized elastoplastic plate theory and its algorithmic implementation," *International Journal for Numerical Methods in Engineering,* vol. 37, pp. 2583-2608, 1994.

[17] J. C. Simo and T. J. Hughes, *Computational Inelasticity*. Secaucus, NJ, USA: Springer-Verlag New York, Incorporated, 1998.

[18] S. M. Kostic*, et al.*, "Evaluation of Resultant Plasticity and Fiber Beam-Column Elements for the Simulation of the 3D Nonlinear Response of Steel Structures," in *2nd International Conference on Computational Methods in Structural Dynamics and Earthquake Engineering - COMPDYN*, Island of Rhodes, Greece, 2009.

[19] F. C. Filippou and G. L. Fenves, "Methods of Analysis for Earthquake-Resistant Structures," in *Earthquake Engineering: From Engineering Seismology to Performance-Based Engineering*, Y. Bozorgnia and V. V. Bertero, Eds., ed: CRC Press, 2004.

[20] F. C. Filippou and M. Constantinides, "FEDEASLab Getting Started Guide and Simulation Examples," University of California, Berkeley, Technical Report2004.

[21] S. M. Kostic and F. C. Filippou, "Section Discretization Considerations in Fiber Beam-Column Elements for Nonlinear Frame Analysis," Pacific Earthquake Engineering Research Center, College of Engineering, University of California, Berkeley (to be published)2010.

[22] M. H. El-Zanaty*, et al.*, "Inelastic behavior of multistory steel frames," Univ. of Alberta, Edmonton, Alberta, Canada Struct. Engrg. Rep. No. 83, 1980.

[23] W. S. King and W. F. Chen, "Practical second-order inelastic analysis of semirigid frames," *J. Struct. Engrg., ASCE,* vol. 120, pp. 2156-2175, 1994.

[24] M. A. Crisfield, *Non-linear finite element analysis of solids and structures*. West Sussex: John Wiley & Sons, 1991.